Synthesis and Characterization of Cerium Molybdate Semiconductor Nanoparticles

Michael Segundo Sena[a]*, Maitê Medeiros de Santana e Silva[a], Andarair Gomes dos Santos[b], André

Luis Lopes-Moriyama[a], Carlson Pereira de Souza[a]

[a]*Department of Graduation in Chemical Engineering, Universidade Federal do Rio Grande do Norte - UFRN, 59.078-970, Natal, RN, Brazil*
[b]*Department of Agrotechnology and Social Sciences, Universidade Federal Rural do Semi-Arido - UFERSA, 59.600-000, Mossoró, RN, Brazil*

Cerium molybdate semiconductive nanoparticles were synthesized by the EDTA-citrate combined complexation method. Gel thermal degradation behavior, phase formation, morphology, composition and band gap of cerium molybdate powders were characterized by TG/DSC, XRD, SEM/EDS and DRS analysis, respectively. The nanoparticles were synthesized by fixing the pH of the reaction medium to 9, producing an organometallic gel which was heated to 230 ºC obtaining a precursor powder. The precursors were calcined in a temperature range of 450 - 800 ºC for 3 h. The cerium molybdate powders were characterized and the phase evolution, morphology and band gap changes with the increase of calcining temperature were investigated. It was observed that the calcining temperature directly influences the formation of the crystalline structure, appearance of other phases in the materials and the particle size.

Keywords: *Cerium molybdate, semiconductors, synthesis by EDTA-Citrate method, optical band gap*

1. Introduction

Cerium molybdate ($Ce_2(MoO_4)_3$) is an important yellow inorganic material of scheelite type with monoclinic crystalline structure that has been extensively studied by the scientific community due to its photoluminescent and photonics properties[1]. It has been used as corrosion inhibitor in metallic alloys[2], photocatalyst in the decomposition of dyes[3], photocatalyst with antibacterial action[4] and many other applications.

Nanostructured semiconductors have been commonly used in optoelectronics and photovoltaic devices, and the interest in investigating the photoelectrochemical properties of these materials have been increased every day[5]. The photocatalytic process is based in a reaction where a semiconductor is activated with light emission with sufficient energy to excite the electrons from the valence band to the conduction band forming an electron-hole pair, the region between the bands is called bandgap.

Many nanomaterials have been explored for applications as photocatalysts with high efficiency. For example, titanium dioxide (TiO_2) nanostructures have been systematically studied and have demonstrated high potential as photocatalysts under UV irradiation[6,7]. However, the limitation of having to work with a wavelength restricted to UV has given rise to new researches in the area, in order to develop materials with promising photocatalytic action within the visible spectrum of light.

Studies have shown that rare earth molybdates with $R_2(MoO_4)_3$ structure, with R= La, Ce, Pr, Nd, Sm e Eu are essentially electronic semiconductors[8]. Besides, rare earth molybdates with optoelectronic and photocatalytic properties have been reported in many publications[5,9,10,11], standing out the cerium molybdate.

The synthesis of cerium molybdate nanostructures has been reported in the literature by several different methods which in turn affect its crystalline structure, such as co-precipitation[12] (amorphous material), hydrothermal[13] ($Ce_2(MoO_4)_3.4.5H_2O$ with unknown crystalline structure), microwave-hydrothermal/solvothermal[1] ($Ce_2(MoO_4)_3$ with unknown crystalline structure), and sol-gel[2] ($Ce(MoO_4)_2$ with tetragonal structure).

Due to the instability of the cerium ion at high temperatures, which can change its oxidation state (Ce^{3+}/Ce^{4+}), there is a certain difficulty in synthesizing a well-crystallized single-phase cerium molybdate with its appropriate crystalline structure, monoclinic symmetry[14]. Hence, the synthesis method has an important role in the structure of the material, and consequently in its electronic properties.

The EDTA-citrate complexing method, a modified Pichine type reaction, is a polymerized complex method to synthesize a wide variety of oxide materials[15]. Ceramic powders are usually synthesized by the conventional solid-state reaction (SSR) method. Compared to SSR method, wet chemical methods, such as EDTA-citrate, is preferable when employing various ceramic materials. The ceramic

*e-mail: michael2.senna@gmail.com.

powders prepared by EDTA-citrate complexing method are calcined at relative low temperature and only requires a short period of time because the reagents are mixed on the molecular scale. The powder produced exhibits small particle size, high specific surface area, uniform element and particle size distribution, which contributes for catalytic and photocatalytic applications[16],[17].

In the present paper, we report for the first time the synthesis of pure crystalline cerium molybdate powders using the EDTA-citrate complexing method at four different calcining temperatures, and we show the phase evolution of the powders, the modifications in the structure, morphology and in the band gap of the material.

2. Materials and Methods

2.1 Synthesis of organometallic precursors

The precursor powders were obtained by EDTA-citrate complexing method. The experimental procedure was given as follows: First of all, EDTA ($C_{10}H_{16}N_2O_8$) was diluted to ammonium hydroxide (NH_4OH) in ratio of 1g:10mL under stirring and controlled temperature (40 ºC). Then, the sources of Ce and Mo cations ($Ce(NO_3)_3.6H_2O$ and $(NH_4)_6Mo_7O_{24}.4H_2O$) were added, maintaining constant temperature and stirring. Then, citric acid ($C_2H_4O_2$) was added and the temperature was increased (80 ºC). The solution pH was adjusted to 9 with addition of ammonium hydroxide, and the solution was maintained under such conditions until formation of the organometallic gel. Then, the gel was pre-calcined to form the precursor powder.

2.2 Samples preparation

Four samples were prepared by calcining the precursors in a muffle furnace at 450, 500, 600 and 800 ºC at a rate of 5 ºC.min^{-1} for 3 h for further analysis.

2.3 Characterizations

2.3.1 Thermogravimetric / differential scanning calorimetry (TG / DSC)

The decomposition behavior of the precursor gel was analyzed by thermogravimetry-differential analysis (TG/DSC, STA 449F3, Netznetzsch) at a heating rate of 5 ºC.min^{-1} up to 1200 ºC for a sample mass of 13.49 mg in alumina crucible.

2.3.2 X-Ray diffraction (XRD)

The phase identification of the synthesized powders, which were calcined at various temperatures, was performed by X-ray diffraction (XRD, D2 Phaser, Bruker) with Cu-Kα ($\lambda = 1.5406$ Å) radiation at a scan rate of 0.01 º.s[-1] in the 2θ range from 10 º to 80 º.

2.3.3 Rietveld refinement

The structural parameters of the powders were obtained by Rietveld refinement analysis of the powder diffraction data using Material Analysis Using Diffraction (MAUD) software version 2.064.

2.3.4 Field emission scanning electron microscopy/ energy dispersive spectroscopy (SEM/EDS)

The morphology of the synthesized powders was determined using a Field Emission Scanning Electron Microscope (FEG SEM, Auriga, Carl Zeiss, USA) operated with an incident electron beam of 30 kV coupled to a microanalysis system of Energy Dispersive Spectroscopy (EDS, SwiftED3000, Oxford Instruments, USA) for quantification and chemical composition analysis. Prior to analysis, the samples were pre-treated, they were suspended in ethanol and dried at 100 ºC for dispertion. Then, the samples were metallized with gold for 30 s and 30 mA in a metallizer (Sputter Coater, SCD 005, Baltec, USA).

2.3.5 Diffuse reflectance spectroscopy (DRS)

The band gap of the powders was analyzed by diffuse reflectance spectroscopy using an UV-Vis spectrophotometer (DRS, 5G, NIR Cary) in the wavelength range 200 - 800 nm, all measurements were performed at room temperature using barium sulfate ($BaSO_4$) as the reference sample for reflectance measurements.

3. Results and Discussion

3.1 Thermogravimetry-differential analysis

Figure 1 illustrates the thermal decomposition behavior of the dried cerium molybdate gel.
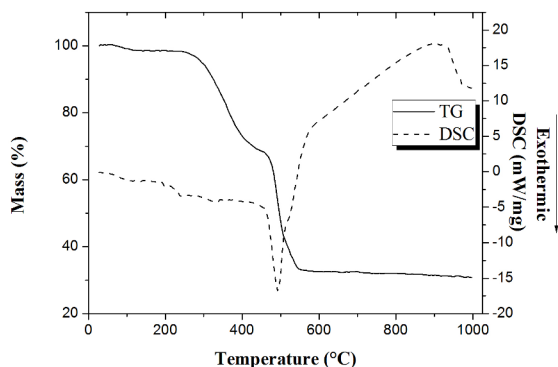

Figure 1. Thermogravimetric analysis curve for cerium molybdate precursors.

The TG of the precursor has three mass-loss steps. In the first step the decomposition occurs between 60 ºC and 130 ºC associated with a weight loss of 2.5 % due to the elimination of residual water and ammonia from the gel[18]. There is also another abrupt weight loss (30 %) in the temperature range 250 - 460 ºC, attributed to the decomposition of the chelates and formation of the organometallic complexes. The third step in the temperature range 460 - 560 ºC is related to a weight loss of 35.58 % and it's followed by a strong and sharp

exothermic peak at 500 ºC on the DSC curve, corresponding to the pyrolysis of the organometallic complex which gives rise to intermediate oxides until formation of crystalline cerium molybdate. Thereafter, there is no further weight loss above 560 ºC, but an endothermic event continues between 560 ºC and 1000 ºC, which indicates that changes in the crystalline structure may occur in this interval.

3.2 Powder X-ray diffraction

As was described by Brazdil (2015)[14], the ideal scheelite structure has a tetragonal unit cell with space group $I\,4_1/a$ (with general formula ABO_4, based on $CaWO_4$) where A^{2+} is a large cation which is 8-coordinated by oxygen, and B^{6+} is a small cation which is tetrahedrally coordinated by oxygen. The incorporation of a trivalent cation in the divalent cation site of the normal scheelite produces a defect structure containing cation vacancies needed for electro-neutrality, crystallizing in a superstructure with monoclinic symmetry, and the resulting empirical formula is $A_2\Upsilon(BO_4)_3$, where Υ indicates a cation vacancy[14]. Furthermore, it stands out that when A cation is cerium there exists optionality for multiple oxidation state (Ce^{3+}/Ce^{4+}).

Figure 2 shows the X-ray diffraction patterns for the cerium molybdate powders calcined in a temperature range of 450-800 ºC.
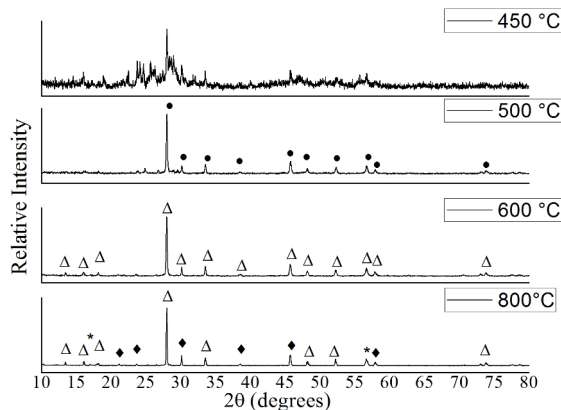

Figure 2. X-ray diffraction patterns of cerium molybdate powders. Symbols legend: ●- tetragonal $Ce_2(MoO_4)_3$, Δ- monoclinic $Ce_2(MoO_4)_3$, ♦- $Ce_{11}O_{20}$, *- Ce_7O_{12}.

The diffractogram of the powders calcined at 450 ºC shows some of the characteristic peaks of cerium molybdate but with many noises and broad peaks, indicating that the material is not completely crystalline. The pattern of the powder calcined at 500 ºC could be indexed to tetragonal $La_2(MoO_4)_3$ (JCPDS card No. 045-04-07). The pattern of the material calcined at 600 ºC could be indexed to monoclinic $La_2(MoO_4)_3$ (JCPDS card No. 01-070-1382), indicating crystalline structure changes of the material as the calcining temperature is increased. This is observed in the sample calcined at 600 ºC from the distinct presence of intense primitive scheelite (tetragonal) diffraction peaks

(28 º - 34 º and 46 º - 58 º), plus the weaker low-angle (10 º - 25 º) superstructure diffraction peaks which are the fingerprints of the defect monoclinic phase[19]. The pattern of the powders calcined at 800 ºC shows the diffraction peaks of the monoclinic phase, but it was also observed the appearance of $Ce_{11}O_{20}$ and Ce_7O_{12} phases due to cerium oxidation. This result was also related by Brazdil et al. (2015)[19] that demonstrated the appearance of CeO_2 phases in the synthesis of cerium molybdate at temperatures above 600 ºC. The diffractograms of the cerium molybdate powders were indexed with lanthanum molybdate cards, as they are isostructural and due to the unavailability of tetragonal and monoclinic cerium molybdate cards in the literature.

3.3 Rietveld refinement

The structural parameters were obtained from Rietveld refinement method using powder XRD data using MAUD software version 2.064. The patterns were typically refined for lattice parameters, unit cell volume and mean crystallite size. The experimental, computed and deviation XRD patterns of $Ce_2(MoO_4)_3$ are shown in Figure 3.

The refinement results show the tetragonal cerium molybdate with space group $I4_1/a$ and the monoclinic cerium molybdate with space group C2/c. The refined structural parameters are summarized in Table 1.

The lattice parameters (a, b, c) shown in Tab. 1 are used to describe the unit cell of the crystalline structure. The results confirm that the material calcined at 500 ºC has a tetragonal structure and the materials calcined at 600 ºC and 800 ºC have monoclinic structure. The lattice parameters obtained in the refinement are very close to the ones of the monoclinic cerium molybdate obtained by Maisang et al. (2016)[1] (a = 16.8762 Å, b = 11.8402 Å, c = 15.9742 Å, β =108.679 º and cell volume = 3023.79 Å³). The results also revealed that the average crystallite size of the particles grew up with increasing temperature, going from 1467.43 Å to 18526.18 Å. The reliability of the data exposed on Tab. 1 is a function of the residual parameter (S), being greater when close to the unity.

3.4 Morphological characterization

Figure 4 shows the SEM images of the cerium molybdate powders synthesized at calcining temperature range of 450 - 800 ºC and heating rate of 5 ºC.min⁻¹.

Fig. 4 (a - d) shows a set of agglomerates of irregularly shaped particles. It is observed that the increase in temperature does not affect the shape of the particles. At 450 ºC, the particles are larger than in the other temperatures, with average size of 328.57 nm. It is due to the fact that there are still carbonates and other organic residues, such as the organometallic complexes formed during the reaction, present in the material composition. These organic residues are completely degraded at about 500 ºC as also confirmed by the TGA measurements in Fig.1, producing carbon monoxide and carbon dioxide, leaving only the oxide of interest in the
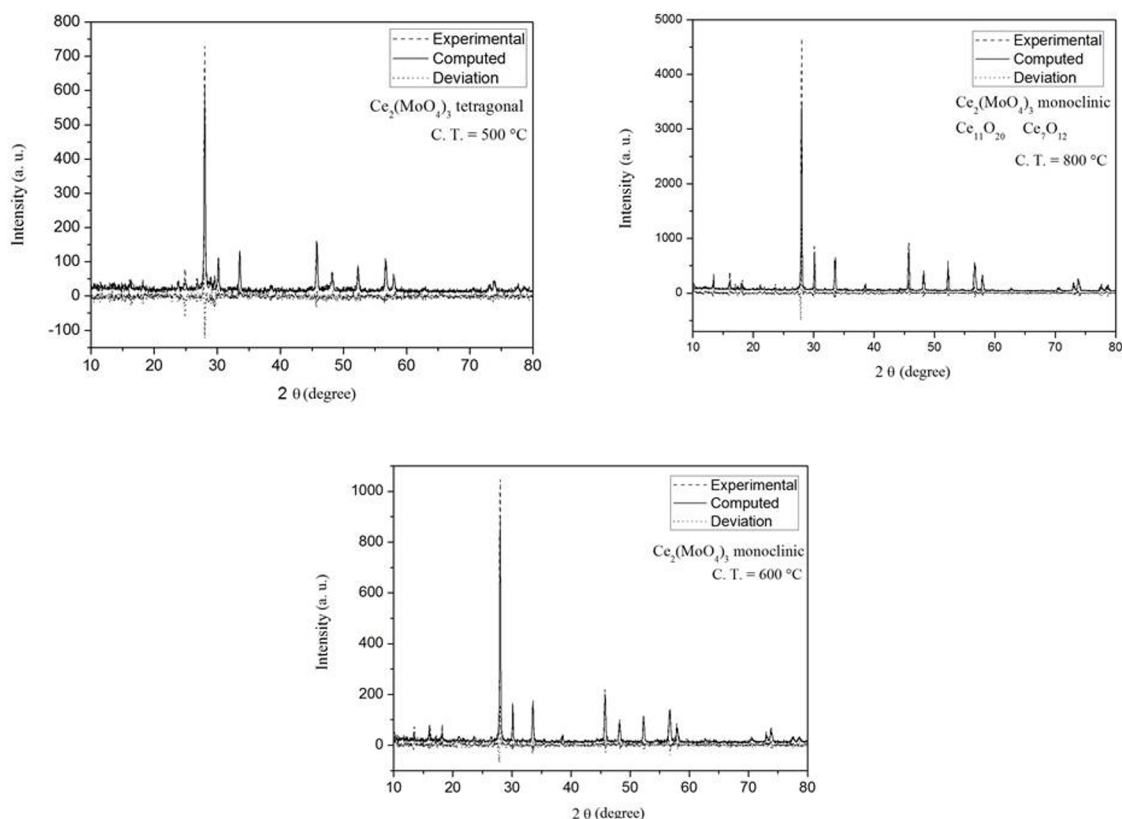
Figure 3. Observed, computed and deviation XRD patterns of $Ce_2(MoO_4)_3$.

Table 1. Lattice parameters, cell volume and average crystallite size from Rietveld refinement of X-ray diffraction data of the samples calcined at 500, 600 and 800 ºC.

Compounds - Calcining temperature	$Ce_2(MoO_4)_3$ - 500 ºC	$Ce_2(MoO_4)_3$ - 600 ºC	$Ce_2(MoO_4)_3$+ cerium oxides - 800 ºC
Crystalline structure	tetragonal	monoclinic	monoclinic
Space group	I41/a	C2/c	C2/c
Lattice parameters			
a (Å)	16.859	16.901	16.877
b (Å)	16.859	11.839	11.840
c (Å)	16.013	15.980	15.976
$\alpha=\gamma$ (º)	90	90	90
β (º)	90	108.487	108.251
Cell volume (Å³)	4550.99	3181.01	3164.03
Average crystallite size (Å)	1467.43	2495.15	18526.18
Residual parameter, S	1.29	1.28	1.98

powder[18], resulting in a material with smaller particle size. The XRD diffractograms previously discussed in Fig.2 also confirm that the material calcined at 450 ºC is not completely crystalline, which is attributed to the presence of organic residues in the composition[18]. At 600 and 800 ºC, it is possible to notice the joining of two or more particles forming larger particles; it is more remarkable at 800 ºC. This phenomenon, within the related temperature, is explained by the decrease

in Gibbs free energy caused by the decrease of the surface area. It is not observed a considerable increase in size of the particles in the temperatures of 500, 600 and 800 ºC, with average size of 159.51, 169.75 and 189.01 nm, respectively.

3.5 Composition analysis

Table 2 shows the EDS results of cerium molybdate samples calcined in the temperature range of 450 - 800 ºC.
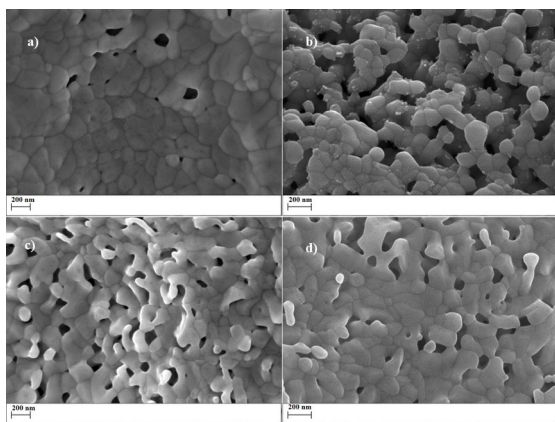
Figure 4. SEM images of cerium molybdate powders (a = 450 ºC; b = 500 ºC; c = 600 ºC; d = 800 ºC).

Table 2. Atomic percentages of Ce and Mo by EDS analysis of cerium molybdate samples calcined in the temperature range 450ºC - 800ºC.

Element	450 ºC	500 ºC	600 ºC	800 ºC
Ce (%)	49.693	45.818	39.231	46.95
Mo (%)	50.307	54.182	60.769	53.05

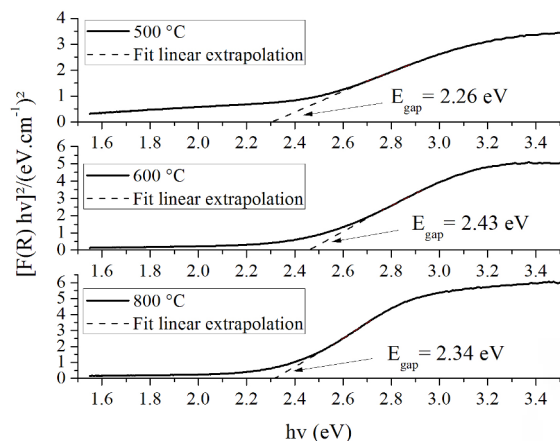**Figure 5.** UV-vis absorbance spectra at room temperature for the $Ce_2(MoO_4)_3$ powders processed EDTA-citrate at 500, 600 and 800ºC for 3 h.

The theoretical atomic composition of $Ce_2(MoO_4)_3$ is 40 % and 60 % of Ce and Mo, respectively, not considering the oxygen in the composition. The presence of Ce and Mo in the samples was confirmed by the EDS analysis. The sample calcined at 600 ºC has the best approximation with the theoretical values, this agrees with the TG and XRD analysis, because the samples calcined at temperatures below 600 ºC did not yield the monoclinic cerium molybdate, and at 800 ºC cerium oxides were yielded which increased the percentage of cerium in relation to molybdenum.

3.6 Optical band gap analysis

The optical energy band gap (E_{gap}) of the as-synthesized $Ce_2(MoO_4)_3$ were estimated from UV-Vis absorption spectra using the equation proposed by Wood-Tauc[20]. According to these researchers, the energy gap (E_{gap}) is related to the absorbance and the photon energy by the Eq (1):

$$\alpha hv = A \left(hv - E_{gap} \right)^n \qquad (1)$$

Where α is the absorbance, A is a proportionality constant, h is the Planck constant, v is the frequency and E_{gap} is the optical band gap, n is a variable that depends on the kind of electronic transition (n = 1/2, 2, 3/2 or 3 for allowed direct, allowed indirect, forbidden direct or forbidden indirect, respectively). Cerium molybdate has been related with direct electronic transition[1], so we considered the value n = 1/2 in Eq (1) for calculating the optical band gap.

Figure 5 show the plots of $(\alpha hv)^2$ versus the photon energy (hv) of the as-synthesized $Ce_2(MoO_4)_3$ calcined at 500, 600 and 800 ºC.

Therefore, the optical band gap was determined by the extrapolation of the linear portion of the curve to zero absorbance. When the photon energy is greater than the energy gap, the absorption linearly increases with the increase of the photon energy. The steep inclination of the linear portion of the curve is caused by the absorption for charge diffusion from the valence band to the conduction band.

The energy difference between the valence and conduction bands is denominated as the band gap characterized by a certain crystal momentum vector in the Brillouin zone. For photon energy smaller than the energy gap, the absorbance curve becomes different from linearity, due to the absorption of charge diffusion relating to different defects[1]. There are several parameters that affect the energy gap such as the electronegativity of transition metal ions, connectivity of the polyhedrons, defects, degree of crystallinity, structure, crystallite size, impurities, product morphologies and others[21].

UV-vis measurements on the three samples showed typical values of E_{gap} = 2.26 eV, 2.43 eV and 2.34 eV for the cerium molybdate samples calcined at 500, 600 and 800 ºC respectively. At 450 ºC, the products are unable to be identified phases which are not able to be compared with the energy gap of the other samples. At 500 ºC the direct energy gap belongs to the tetragonal phase of $Ce_2(MoO_4)_3$ which is smaller than the direct energy gap of the monoclinic phase of $Ce_2(MoO_4)_3$ synthesized at 600 ºC. And the sample calcined at 800 ºC, the direct energy gap belong to the mixed phases of $Ce_2(MoO_4)_3$, $Ce_{11}O_{20}$ and Ce_7O_{12}. The changes in the crystal structure are the reason for the differences in the energy gap values of the samples. These E_{gap} values classify the nanoparticles as semiconductor materials and are very close to E_{gap} = 2.55 eV calculated for cerium molybdate synthesized by solvothermal method[3] and values between E_{gap} = 2.30 and 2.80 eV for cerium molybdate synthesized by microwave-hydrothermal/solvothermal method[1].

4. Conclusions

Cerium molybdate nanoparticles have been successfully synthesized by EDTA-citrate complexing method. The data revealed the structure change and appearance of cerium oxides phases with increasing temperature, the results show the optimal calcining temperature to obtain a well-crystallized single-phase material by this method at about 600 ºC, which was confirmed through thermal, structural and elemental analysis. XRD patterns revealed that the material calcined at 450 ºC is not completely crystalline and exhibit single tetragonal structure at 500 ºC, single monoclinic structure at 600 ºC, and with subsequent increase of temperature to 800 ºC, cerium oxides phases appear in the monoclinic structure. Rietveld refinement revealed the structural parameters of the samples, space group, lattice parameters and main crystallite size. SEM images of the materials calcined at the temperature range of 450 - 800 ºC showed a set of agglomerates of irregularly shaped particles. The increase in heat treatment temperature does not affect the shape of the particles, but affects its size. The composition analysis revealed that the material calcined at 600 ºC has the closest atomic composition of the theoretical atomic composition of pure cerium molybdate ($Ce_2(MoO_4)_3$). Ultraviolet-visible absorption spectroscopy revealed a characteristic optical band gap of 2.26 eV, 2.43 eV and 2.34 eV for the materials calcined at 500 ºC, 600 ºC and 800 ºC, respectively, which is associated with the difference of energy between the valence band and conduction band, classifying the nanoparticles as semiconductors. The photocatalytic potential of cerium molybdate synthesized by EDTA-citrate method will be evaluated by the degradation of organic dyes under UV light irradiation for further publications.

5. Acknowledgments

6. References

1. Maisang W, Phuruangrat A, Thongtem S, Thongtem T. Photoluminescence and photonic absorbance of $Ce_2(MoO_4)_3$ nanocrystal synthesized by microwave-hydrothermal/ solvothermal method. *Rare Metals.* 2016 DOI: 10.1007/s12598-016-0714-7

2. Kartsonakis IA, Kordas G. Synthesis and Characterization of Cerium Molybdate Nanocontainers and Their Inhibitor Complexes. *Journal of the American Ceramic Society.* 2010;93(1):65-73.

3. Ayni S, Sabet M, Salavati-Niasari M, Hamadanian M. Synthesis and characterization of cerium molybdate nanostructures via a simple solvothermal method and investigation of their photocatalytic activity. *Journal of Materials Science: Materials in Electronics.* 2016;27(7):7342-7352.

4. Kartsonakis IA, Kontogiani P, Pappas GS, Kordas G. Photocatalytic action of cerium molybdate and iron-titanium oxide hollow nanospheres on *Escherichia coli. Journal of Nanoparticle Research.* 2013;15(6):1759.

5. Kwolek P, Pilarczyk K, Tokarski T, Łapczyńska M, Pacia M, Szaciłowski K. Lead molybdate - a promising material for optoelectronics and photocatalysis. *Journal of Materials Chemistry C.* 2015;3(11):2614-2623.

6. Kaur K, Pal B. Selective formation of benzo[c]cinnoline by photocatalytic reduction of 2,2'-dinitrobiphenyl using TiO_2 and under UV light irradiation. *Chemical Communications.* 2015;51(40):8500-8503.

7. Li JR, Yang CH, Wu LG, Cao YQ, Wang T, Jiang BQ. Enhancement on the performance of TiO_2 photocatalysts under weak UV light irradiation via asorbed-layer nanoreactor technique. *Colloids and Surfaces A: Physicochemical and Engineering Aspects.* 2015;481:413-422.

8. Gaur K, Singh M, Lal HB. Electrical transport in light rare-earth molybdates. *Journal of Materials Science.* 1993;28(14):3816-3822.

9. Dutta S, Som S, Priya J, Sharma SK. Band gap, CIE and trap depth parameters of rare earth molybdate phosphors for optoelectronic applications. *Solid State Sciences.* 2013;18:114-122.

10. Edrissi M, Samadanian-Isfahani S, Soleymani M. Preparation of cobalt molybdate nanoparticles; Taguchi optimization and photocatalytic oxidation of Reactive Black 8 dye. *Powder Technology.* 2013;249:378-385.

11. Yousefi T, Khanchi AR, Ahmadi SJ, Rofouei MK, Yavari R, Davarkhah R, et al. Cerium(III) molybdate nanoparticles: Synthesis, characterization and radionuclides adsorption studies. *Journal of Hazardous Materials.* 2012;215-216:266-271.

12. Yasakau KA, Tedim J, Zheludkevich ML, Drumm R, Shem M, Wittmar M, et al. Cerium molybdate nanowires for active corrosion protection of aluminium alloys. *Corrosion Science.* 2012;58:41-51.

13. Dong M, Lin Q, Sun H, Chen D, Zhang T, Wu Q, et al. Synthesis of Cerium Molybdate Hierarchical Architectures and Their Novel Photocatalytic and Adsorption Performances. *Crystal Growth & Design.* 2011;11(11):5002-5009.

14. Brazdil JF. Scheelite: a versatile structural template for selective alkene oxidation catalysts. *Catalysis Science & Technology.* 2015;5(7):3452-3458.

15. Ding X, Liu Y, Gao L, Guo L. Synthesis and characterization of doped $LaCrO_3$ perovskite prepared by EDTA-citrate complexing method. *Journal of Alloys and Compounds.* 2008;458(1-2):346-350.

16. Cao Y, Zhu K, Zheng H, Qiu J, Gu H. Synthesis of potassium sodium niobate powders using an EDTA/citrate complexing sol-gel method. *Particuology.* 2012;10(6):777-782.

17. Hung IM, Chiang YJ, Lee SW, Chang JK, Lin JC, Jang JSC, et al. Material characterization and electrochemical performance of $Sr(Ce_{0.6}Zr_{0.4})_{0.8}Y_{0.2}O_{3-\delta}$ proton conducting ceramics prepared by EDTA-citrate complexing and solid-state reaction methods. *Journal of the Ceramic Society of Japan.* 2015;123(1436):187-192.

18. Patra H, Rout SK, Pratihar SK, Bhattacharya S. Effect of process parameters on combined EDTA-citrate synthesis of $Ba_{0.5}Sr_{0.5}Co_{0.8}Fe_{0.2}O_{3-\delta}$ perovskite. *Powder Technology.* 2011;209(1-3):98-104.

19. Brazdil JF, Toft MA, Lin SSY, McKenna ST, Zajac G, Kaduk JA, et al. Characterization of bismuth-cerium-molybdate selective propylene ammoxidation catalysts. *Applied Catalysis A: General.* 2015;495:115-123.

20. Wood DL, Tauc J. Weak Absorption Tails in Amorphous Semiconductors. *Physical Review B.* 1972;5(8):3144-3151.

21. Keereeta Y, Thongtem T, Thongtem S. Synthesis of lanthanum tungstate interconnecting nanoparticles by high voltage electrospinning. *Applied Surface Science.* 2015;351:1075-1080.